Role of photonic bandgaps in polarization-independent grating waveguide structures

Eran Grinvald,[1,*] Tsvi Katchalski,[1] Silvia Soria,[2] Shimon Levit,[1] and Asher A. Friesem[1]

[1]*Weizmann Institute of Science, Rehovot 76100, Israel*
[2]*Centro Studi e Ricerche Enrico Fermi–IFAC Institute of Applied Physics, 500019 Sesto Fiorentino, Italy*
[*]*Corresponding author: eran.grinvald@weizmann.ac.il*

Received November 2, 2007; revised April 6, 2008; accepted April 8, 2008;
posted April 17, 2008 (Doc. ID 89313); published May 29, 2008

Polarization independence in a one-dimensional resonant grating waveguide structure involves the simultaneous excitation of two guided modes propagating in different directions. Possible simultaneous excitations occur when the two excited guided modes have either the same polarization, i.e., TE–TE (transverse electric) or TM–TM (transverse magnetic), or different polarizations, i.e., TE–TM. Simultaneous excitations may result in bandgaps and singularities. We confirm and show that in order to achieve polarization independence, it is necessary to find the conditions that minimize the effects of such bandgaps and singularities and experimentally demonstrate tunable polarization independence for simultaneously excited TE–TM-guided modes.

OCIS codes: 050.5745, 230.3120, 230.7400, 350.4238.

1. INTRODUCTION

Resonant grating waveguide structures (GWSs) are multilayered structures that exhibit an anomaly in the reflected light at a specific wavelength, angular orientation, and polarization of the incident light when radiating guided modes are excited [1]. Although in general the resonant response of a GWS depends on polarization, special GWS geometries and incident illumination conditions were found to yield polarization independence. These include one-dimensional GWSs with specific grating duty cycles that are illuminated at a full conical incidence angle [2–4], as well as two-dimensional GWSs with specifically chosen grating parameters that are illuminated at normal incidence [5,6] or oblique incidence [7–9].

In this paper we show that polarization independence need not be confined to these special cases. Indeed, there is a range of incident angular orientations for which there is a corresponding range of wavelengths that will lead to near-polarization-independent resonance for any one-dimensional GWS. In our approach we characterize the GWS by photonic bands that are formed by plotting the reflection efficiencies as a function of the angular orientation and wavelength of the incident light at resonance. We will demonstrate that near polarization independence is possible when the photonic bandgaps between the bands are relatively small in frequency and the polarizations of the two bands around the gap are nearly orthogonal. With this development, the GWS becomes more attractive for a number of applications that require high spectral resolution and nonpolarized light, including sensitive biological/chemical sensors [10,11] and optical communications [12–14].

We begin by using wave-vector diagrams (WVDs) [15,16] in order to find the approximate resonant wavelength and angular orientation of the incident beam where two different directional guided modes are simultaneously excited and then resort to more accurate and exact numerical rigorous coupled-wave analysis (RCWA) calculations [17], which take into account mode coupling and polarization effects. We consider and compare polarization independence in one-dimensional GWSs when the two simultaneously excited radiating guided modes are of the same polarization as well as when their polarizations differ and qualitatively compare the two situations. Finally, we experimentally demonstrate tunable near-polarization-independent behavior when the polarizations of the excited modes differ.

2. DESIGN CONSIDERATIONS

The basic GWS configuration, together with the relevant geometrical and optical parameters that affect the resonance, is presented in Fig. 1. The GWS is composed of a waveguide layer of thickness h_{wg} and dielectric index ϵ_{wg}, a grating layer of thickness h_{gr}, period Λ, grating duty cycle a/Λ, and dielectric index ϵ_{gr}. These layers are deposited on a thick substrate of dielectric index ϵ_{sb}. On top of the GWS there is a superstrate layer of dielectric index ϵ_{sp}, usually air. Also shown are two alternative representations of the angular orientation of the incident light beam. In one, shown in Fig. 1(a), the angular orientation is denoted by a set of two "spherical coordinate" angles; φ, the angle between the plane of incidence in respect to the x axis; and θ, the angle between the incident light beam and the z axis. In the other, shown in Fig. 1(b), the angular orientation is denoted by a set of "cartesian" angles: θ_C denotes the classical orientation where the plane of incidence is perpendicular to the grating grooves (initial ro-

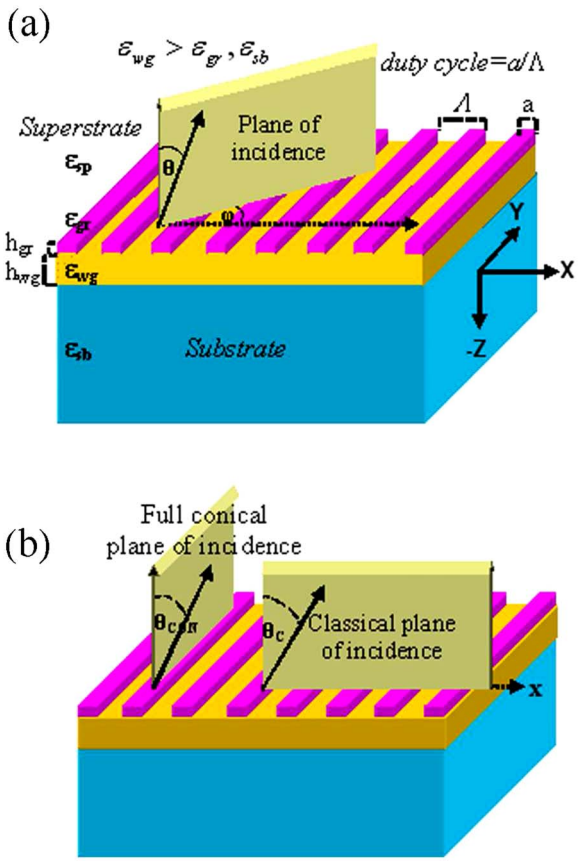

Fig. 1. (Color online) Basic GWS configuration with geometrical and optical parameters and incident light orientation denoted by (a) "spherical" angles φ and θ. A specific plane of incidence is defined by the value of φ. (b) "Cartesian" angles θ_C along the classical plane of incidence and θ_{CON} along the full conical plane of incidence.

tation around the y axis), and θ_{CON} denotes the conical angle where the plane of incidence is along the grooves (initial rotation around the x axis). In essence, θ_C denotes the angle between the propagation vector of the incident light beam and its projection on the y–z plane, while θ_{CON} denotes the angle between the propagation vector of the incident light beam and its projection on the x–z plane. The relation between the two sets of angles is

$$\sin(\theta_C) = \sin(\theta)\cos(\varphi),$$

$$\sin(\theta_{CON}) = \sin(\theta)\sin(\varphi). \quad (1)$$

Since the grating in a GWS is periodic in the x direction, we can resort to the Bloch–Floquet condition [15] to write the resonance condition for the excitation of a guided mode of the structure without the grating. This yields a wave vector $\beta_{TE/TM}$ for either transverse electric (TE) or transverse magnetic (TM) polarization of the form

$$\beta_{TE/TM}^2 = (k_x - mK_x)^2 + k_y^2, \quad (2)$$

where K_x denotes the basic reciprocal lattice constant of the grating, $K_x = 2\pi/\Lambda$; Λ is the grating period; m is the diffracted order; and k_x and k_y are the transverse incident wave vectors in the x and y directions, respectively. The incident wave vectors k_x and k_y are related to the angular

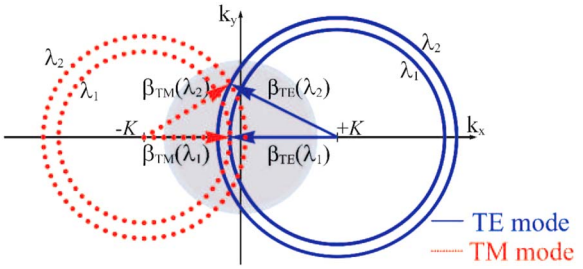

Fig. 2. (Color online) Wave-vector diagrams showing conditions for which TE- and TM-guided modes are simultaneously excited at classical (λ_1) and off-classical (λ_2) incidence.

orientation of the incident light θ_C and θ_{CON} by $k_x = k_0 \sin(\theta_C)$ and $k_y = k_0 \sin(\theta_{CON})$, where $k_0 = 2\pi/\lambda_0$ is the free-space wave vector with λ_0 the free-space wavelength. The corresponding set of spherical coordinate angles φ and θ can be found from Eqs. (1).

Equation (2) represents circles centered at $(mK_x, 0)$ and can be drawn as WVDs [2] when letting the frequency of the guided mode be equal to that of the incident light. A representative WVD for first-order diffractions $m = \pm 1$ is shown in Fig. 2. Here the circles are centered at $+K_x$ and $-K_x$ with radii $\beta_{TE}(\lambda_1)$ and $\beta_{TM}(\lambda_1)$ corresponding to wavelength λ_1 and $\beta_{TE}(\lambda_2)$ and $\beta_{TM}(\lambda_2)$ corresponding to λ_2, where the circles on the right correspond to TE-excited guided modes and those on the left to TM. The central gray circular area represents a light cone, which has a radius of k_o. Only those guided modes with wave vectors β_{TE} or β_{TM} that fall on the arcs within the light cone can be excited.

The intersections for circles with the same wavelength indicate where two guided modes are simultaneously excited, each with corresponding wave vectors as shown in Fig. 2. Such simultaneous excitation is necessary [2,8] but not sufficient for polarization independence [4]. At classical incidence, i.e., $k_y = 0$, an intersection occurs at the point where the TM circle touches tangentially the TE circle for incident wavelength λ_1. When the size of the circles increases, i.e., for a shorter wavelength ($\lambda_2 < \lambda_1$), intersections will occur at off-classical incidence. On the other hand, for longer wavelengths ($\lambda_2 > \lambda_1$), there are no intersections, indicating the absence of simultaneously excited guided modes and no possibility for polarization independence. It should be noted that the WVDs do not take into account mode coupling nor the finite bandwidth of the resonance, both of which allow the coupling of guided modes and incident light of different frequencies. These will effectively lead to the widening of the circumference of the WVD circles and possible splitting at the intersections [15,16].

3. CALCULATED RESULTS

In order to take into account the coupling between the incident light and the excited guided modes, as well as the coupling between two simultaneously excited guided modes, we resorted to numerical calculations based on the RCWA method for infinite gratings [17,18]. Specifically, we calculated the reflection efficiency as a function of the angular orientation and wavelength of the incident light. For these calculations we used the "Cartesian" set, θ_{CON}

and θ_C, to denote the angular orientation of the incident light, as they are closely related to k_x and k_y, making the comparison between WVDs and exact numerical calculations direct. The Cartesian set is also closely related to our experimental setup, where we change the angular orientation by rotating the GWS around two perpendicular axes. In addition, each angle represents a variation along a different symmetry axis of the GWS; specifically, the homogeneous axis y for which the k_y of the incident light and excited guided mode must be the same, and the periodic axis x for which the k_x of the incident light and excited guided mode will vary by $\pm K_x$. For these and all subsequent calculations and experiments, we used a typical GWS having the following parameters: Waveguide layer of 0.47 μm thickness and refractive index $n=1.75$, grating of 0.980 μm period, 0.35 μm thickness, $n=1.55$, 50% duty cycle (unless specified otherwise), superstrate of $n=1$, and substrate of $n=1.5$.

The calculated results are presented in Figs. 3–7. We begin by summarizing the polarization-independent resonant behavior when two excited guided modes with the same polarization, i.e., TM–TM and TE–TE, are excited, confirming earlier theoretical [2,4,8] and experimental results [3]. Specifically, we calculated the reflection efficiency as a function of the full conical angular orientation (since simultaneous excitation of two guided modes of the same polarization and order always occurs at $\theta_C=0°$) and the wavelength for right-handed circularly polarized, s-polarized, and p-polarized incident light. The results are presented in Fig. 3. Figure 3(a) shows two main resonance bands when the incident light is circularly polarized, a TE–TE resonance band at long wavelengths, and a TM–TM band at short wavelengths. A close examination reveals that each band is actually composed of two separated "inner" bands displaced by a small photonic bandgap. The two bands result from the in-phase and out-of-phase excitation of the simultaneously excited modes,

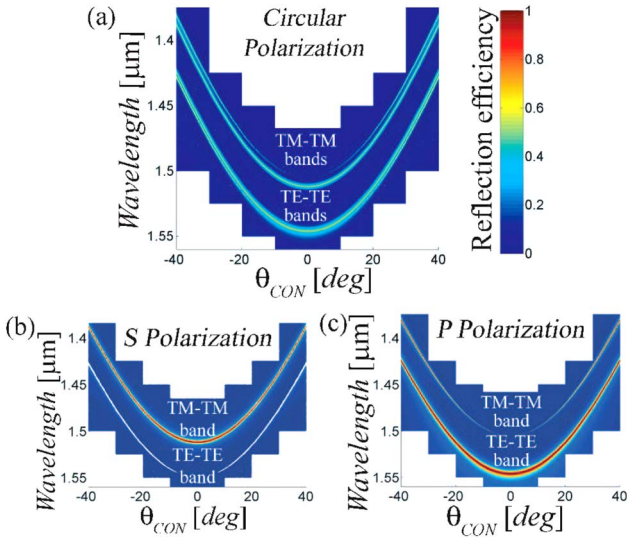

Fig. 3. (Color online) Numerically calculated reflection efficiency as a function of full conical incidence angle θ_{CON} and the wavelength for TM–TM- and TE–TE-excited guided modes. (a) Circularly polarized incident light, (b) s-polarized incident light, (c) p-polarized incident light. (See color online for details of color-coded reflection efficiency.)

which generally have different field distributions in the high and low refractive index regions of the grating [19–21]. As evident in Fig. 3(a), the reflection efficiency is relatively low in these bands, indicating that there is no efficient polarization independence.

Figure 3(b) shows that only one of the TM–TM separated bands and only one of the TE–TE separated bands are excited when the incident light is s polarized. Figure 3(c) shows that the other band of the TM–TM separated bands and the other band of the TE–TE separated bands are excited when the incident light is p polarized. Thus, each of the TM–TM separated bands and each of the TE–TE separated bands are excited by incident light of orthogonal polarizations, and no polarization independence is possible when there is a gap between the separated bands. Moreover, Figs. 3(b) and 3(c) reveal that at normal incidence, there is no resonance in one of the TM–TM separated bands and in one of the TE–TE separated bands because of a singularity. Thus, no polarization independence is possible with 1D gratings illuminated at normal incidence. Efficient polarization-independent resonance is also not possible at small conical angles, due to the very different bandwidths of the s and p resonances in the bands with and without the singularity. Nevertheless, by tailoring the duty cycle to very specific values, it was shown that tunable polarization independence can be obtained at large angles of full conical incidence [3]. From our point of view, tailoring the duty cycle leads to elimination of the bandgap and polarization independence.

To summarize, TE–TE and TM–TM resonances always occur on a symmetry axis of the GWS, i.e., $k_x=0$ for a 1D GWS. Such resonances usually result in photonic bandgaps, where each of the bands is excited by either only s or only p polarization. This means that efficient polarization-independent resonance occurs only for specifically designed GWSs, where there is no bandgap.

Unlike TE–TE and TM–TM resonances that always occur on a symmetry axis of the GWS, i.e., full conical incidence, TE–TM resonance occurs on a symmetry axis of the GWS, i.e., classical incidence, for only a single wavelength. The TE–TM resonance at classical incidence is polarization independent [22] for any GWS because there is no coupling between the counter propagating TE and TM modes and thus no bandgap, as the bands always cross. Like the TE–TE and TM–TM resonances, the wavelength of the TE–TM resonance can be tuned by changing the angular orientation of the incident light. However, this occurs at a general incidence orientation with no symmetry properties, indicating that the polarization of the incident light at resonance is no longer either only s or only p, as it is in classical or full conical incidence. To the best of our knowledge, this paper is the first to study TE–TM simultaneous excitation off-classical incidence.

Figure 4 shows the reflection efficiency of right-handed circularly polarized incident light as a function of the classical θ_C and conical θ_{CON} incident angles around which TE–TM simultaneous guided modes are excited at two specific wavelengths. One wavelength is $\lambda_1=1.528$ μm, where polarization independence is at classical incidence, and the other wavelength $\lambda_2=1.512$ μm was chosen to be lower than λ_1. The regions of "intersections"

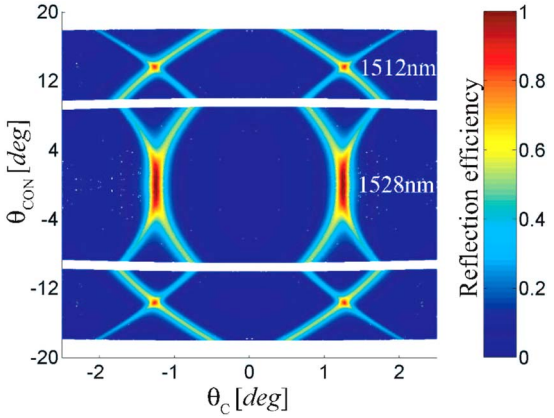

Fig. 4. (Color online) Numerically calculated reflection efficiency of right-handed circularly polarized incident light as a function of θ_{CON} and θ_C, for two wavelengths $\lambda_1=1.528\ \mu$m and $\lambda_2=1.512\ \mu$m, and TE–TM-excited guided modes. Near polarization independence occurs at intersections. (See color online for details of color-coded reflection efficiency.)

in Fig. 4 essentially correspond to the magnified regions of intersection in Fig. 2. The results of Fig. 4 reveal that the reflection efficiency, denoted by the gray-scale code, is highest where the TE and TM circular bands intersect, rising from under 60% away from the crossing to over 80% around the crossing. For $\lambda_1=1.528\ \mu$m, where the circular bands are tangential to each other, the angular tolerance for maintaining polarization independence is small for deviations along the classical angle θ_C but is relatively large for deviations along the conical angle θ_{CON}. For $\lambda_2=1.512\ \mu$m, it seems at first glance that polarization independence can still be obtained where the circular bandsintersect, but with decreased conical angular tolerance.

From the results of Fig. 4 it is difficult to clearly see the details of the resonance in the intersection regions, because the width of each band is comparable to or greater than the size of the intersection. Thus, in order to obtain more details, we performed RCWA calculations around the intersection regions. Specifically, we calculated the angular orientations of the incident light at which the reflection efficiency is 99.99% or more as a function of the incident light for several representative polarizations. The results are presented in Fig. 5. They show the reflection efficiency as a function of angular orientations of the incident light for four different grating duty cycles. At each duty cycle we chose a corresponding wavelength so that the TE and TM bands will "intersect" at similar angular orientations of the incident light. Two bands around the intersections are shown, where each segment of the bands corresponds to a different incident light polarization. The star in each graph denotes the location of the angular orientation of the incident light at which maximal average reflection efficiency for two orthogonal polarizations is obtained. This location does not depend on the specific pair of orthogonal polarizations.

The polarization of the incident light is denoted by the parameter set (α,β), where α is the orientation of the principal polarization axis of the electric field (when $\alpha=0°$, the polarization axis is perpendicular to the plane of incidence, i.e., *s*-polarized light) and β is the degree of ellipticity of the polarization. In our notation, $\tan(\beta)=E_2/E_1$, where E_1 is the electric field along the principal polarization axis and E_2 is that along the secondary axis. For such elliptic polarizations, E_1 and E_2 are always 90° out of phase. Thus, $\beta=0°$ corresponds to linearly polarized light, while $\beta=\pm45°$ corresponds to right- or left-handed circularly polarized light.

Figure 5(a) shows the results for a grating duty cycle of 50% and $\lambda=1.512\ \mu$m. As is evident, a gap along the θ_C direction is clearly observed. The gap corresponds to a split of the "crossing" for the λ_2 circles of the WVD shown in Fig. 2. Such an angular gap along the k_x direction, namely, the k gap/momentum gap, has been noted for surface plasmon resonance [23–25] as well as for guided-mode resonance [26]. The k gaps usually occur when the direct coupling between the two excited modes [26] is much weaker than the coupling to the radiation modes, as is the case between our TE and TM modes, whose electric fields are almost orthogonal. Within a k gap, the reflection efficiency at any arbitrary wavelength is always less than 100%. Far from the gap, the top of the left band and the bottom of the right band correspond to TE-excited guided modes at resonance, as can be inferred from crossings of the large TE circle with the smaller TM circle in WVDs at positive angular orientations. Near the gap, there is simultaneous excitation of TE- and TM-guided modes at resonance, just as there would be in any two-level resonant system. Note that the incident polarization at the lower-left and upper-right bands where TM is dominant does not vary as much as the other parts of the bands where TE is dominant.

Figure 5(b) shows the results for a grating duty cycle of 41.63% and $\lambda=1.508\ \mu$m. For this grating duty cycle there is no angular bandgap, but unlike at TE–TE or TM–TM crossings where the resonant incident polarizations of the two bands are orthogonal [2,3,8], at this TE–TM crossing they converge to the same polarization. As is evident, the polarization of the band where TE is dominant remains essentially constant around the crossing, while the polarization of the band where TM is dominant varies greatly.

Figure 5(c) shows the results for a grating duty cycle of 25% and $\lambda=1.503\ \mu$m. An angular gap along the θ_{CON} direction is clearly observed. It is fundamentally different from the gap of Fig. 5(a), as it is along the k_y direction, which corresponds to a frequency gap. Within a k_y gap, the reflection efficiency at the top band (larger θ_{CON}) can reach 100% for a resonant wavelength higher than $1.503\ \mu$m, and at the lower band it can reach 100% for a resonant wavelength lower than $1.503\ \mu$m. Thus, for the specific wavelength of $1.503\ \mu$m we obtain a k_y gap, while for a specific angular orientation we obtain a frequency gap. At about $\theta_C=1.34°$, where the bandgap is minimal, the polarizations at the top and bottom of the gap are not orthogonal. This suggests that unlike for TE–TE and TM–TM simultaneous excitations, for TE–TM simultaneous excitation the absence of a bandgap is not a sufficient condition for complete polarization independence.

Figure 5(d) shows the results for a grating duty cycle of 47.2% and $\lambda=1.5105\ \mu$m. For the GWS parameters used in this paper, at this grating duty cycle we obtained the highest possible average reflection efficiency of 93% for two orthogonal polarizations and similar angular orienta-

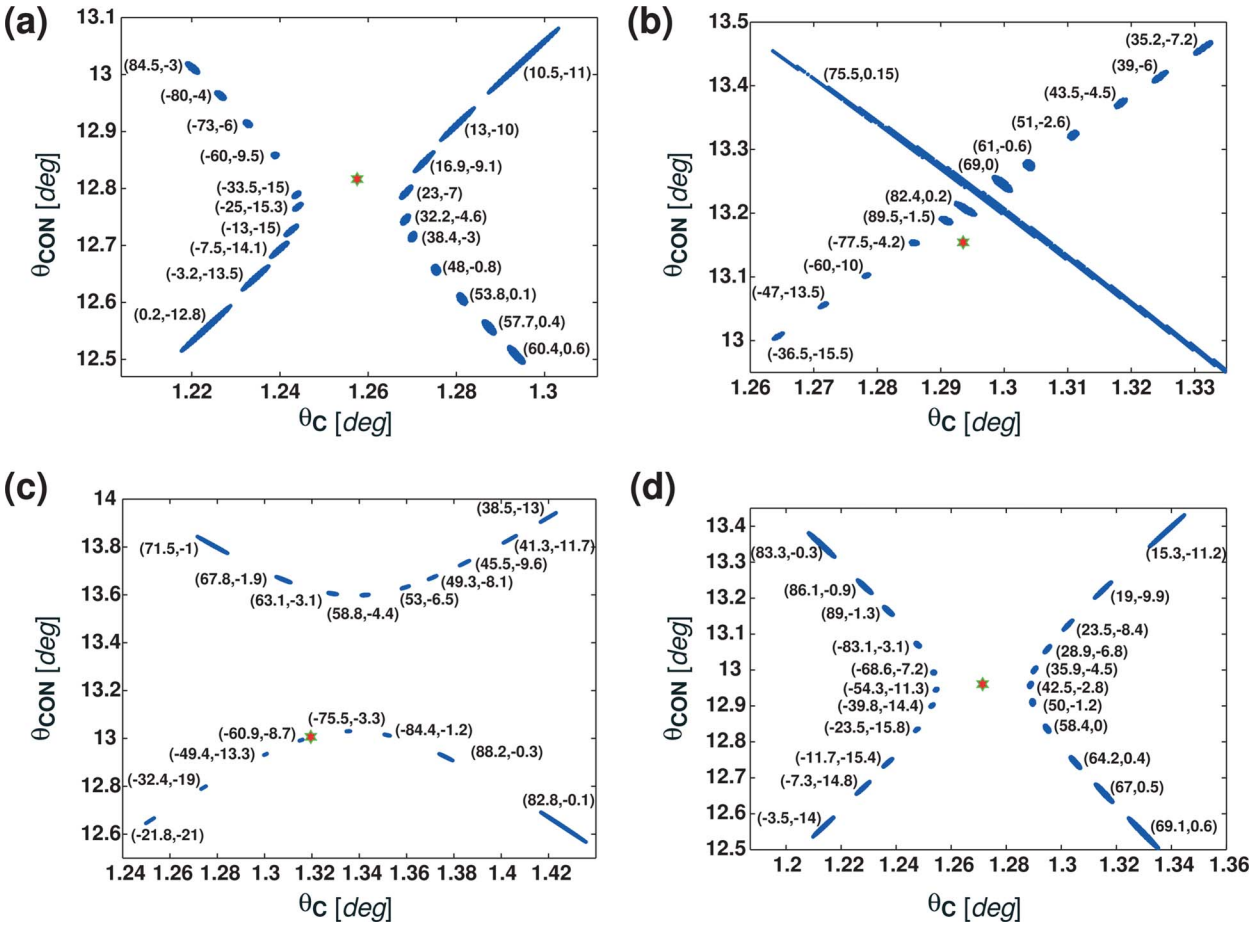

Fig. 5. (Color online) Numerically calculated angular orientations of the incident light at which the reflection efficiency is 99.99% or more, revealing the angular band structures for four different duty cycles and the corresponding wavelengths. Each segment of the bands is calculated for a different incident light polarization, as labeled. In each figure the star denotes the angular orientation of the incident light at which maximal average reflection efficiency is obtained for two orthogonal polarizations: (a) 50% grating duty cycle and $\lambda = 1.512\ \mu$m, where a k gap is evident; (b) 41.63% grating duty cycle and $\lambda = 1.508\ \mu$m, where a band crossing is evident; (c) 25% grating duty cycle and $\lambda = 1.503\ \mu$m, where a k_y gap corresponding to a frequency bandgap is evident; (d) 47.2% grating duty cycle and $\lambda = 1.5105\ \mu$m, where a k gap is evident.

tions of the incident beam. The results show a k gap similar to the one in Fig. 5(a) except that here there is more symmetry. Specifically, the polarization variations along the bands where TE is dominant and where TM is dominant are now similar, the resonant polarizations at both edges of the gap are essentially orthogonal, and the maximal average reflection efficiency for the two orthogonal polarizations occurs exactly at the center of the gap.

We now consider in more detail the polarization behavior where the highest average reflection efficiencies are obtained, i.e., at the locations of the stars in Fig. 5. Specifically, using RCWA we calculated the reflection efficiency as a function of the polarization of the incident light $[\alpha, \beta]$, at the specific wavelengths and angular orientations of the incident light for the four different grating duty cycles. The gray-scale-coded (see color-coded scale online for more details) results are presented in Fig. 6. As evident, except for a grating duty cycle of 25%, the reflection efficiencies are high and relatively constant for all polarizations. For example, for a grating duty cycle of 50% [Fig. 6(a)] the average reflection efficiency and the maximal deviations are $91.5\% \pm 7.5\%$, for a grating duty cycle of 41.63% [Fig. 6(b)] they are $87\% \pm 13\%$, for a grating

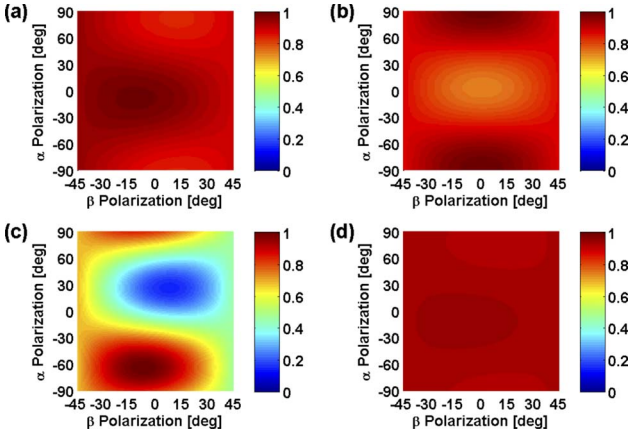

Fig. 6. (Color online) Numerically calculated gray-scale-coded reflection efficiency as a function of the polarization of the incident light $[\alpha, \beta]$ for the same four duty cycles and wavelengths of Fig. 5. The results are for the angular orientation denoted by a star in Fig. 5. The average reflection efficiency and maximal deviations are (a) $91.5\% \pm 7.5\%$ at $[\theta_C, \theta_{CON} = 1.26°, 12.82°]$; (b) $87\% \pm 13\%$ at $[1.29°, 13.15°]$; (c) $57.5\% \pm 42.5\%$ at $[1.32°, 13.01°]$; (d) $93\% \pm 1.5\%$ at $[1.27°, 12.96°]$. (See color online for details of color-coded reflection efficiency.)

duty cycle of 47.2% [Fig. 6(d)] they are 93% ± 1.5%, and for a grating duty cycle of 25% [Fig. 6(c)] they are 57.5% ± 42.5%. The highest average reflection efficiency of 93% is obtained for the grating duty cycle of 47.2%, even though the maximal reflection efficiency with this grating duty cycle is lower than with the others. It should be noted that, surprisingly, the average reflection efficiency for the grating duty cycle of 41.63% where the bands cross [Fig. 6(b)] is lower and the maximal deviation higher than for the two grating duty cycles [Figs. 6(b) and 6(d)] where there is a k gap.

As can be determined from Fig. 6, the maximal and minimal reflection efficiencies at each of the grating duty cycles are as follows: For a grating duty cycle of 50%, maximal reflection efficiency is 99% at $(\alpha,\beta)=(-12,-9)$, and minimal is 84% at $(\alpha,\beta)=(78,9)$; for 41.63%, maximal reflection efficiency is 99.5% at $(\alpha,\beta)=(87,0)$, and minimal is 74% at $(\alpha,\beta)=(-3,0)$; for 25%, maximal reflection efficiency is 100% at $(\alpha,\beta)=(87,0)$, and minimal is about 15% at $(\alpha,\beta)=(-3,0)$; for 47.2%, maximal reflection efficiency is 94.5% at $(\alpha,\beta)=(-12,-9)$, and minimal is 91.5% at $(\alpha,\beta)=(78,9)$. These results indicate that the polarizations for maximal and minimal reflection efficiencies are essentially orthogonal, in accordance with the orthogonality condition of $\alpha_1-\alpha_2=\pm 90°$ and $\beta_1=-\beta_2$.

Using the maximal and minimal polarizations from Fig. 6 and the same angular orientations (location of the stars in Fig. 5), we also calculated the reflection efficiencies as a function of wavelength of the incident light. The results are presented in Fig. 7 along with those calculated for classical incidence of the TE–TM crossings that occur at higher wavelengths. The wavelengths for which the maximal and minimal polarizations were obtained and used in Figs. 5 and 6 are denoted by diamonds along the abscissa. The results at classical incidence are for *s* and *p* incident polarizations corresponding to TE- and TM-excited guided modes, respectively. A different pair of two orthogonal polarizations would only change the bandwidths of the two resonances. As evident in Figs. 7(a)–7(d), the resonances that occur for classical incidence at the intersection region are indeed polarization independent, exhibiting 100% reflection for both orthogonal polarizations at the same wavelength. In general, the spectral bandwidths are not identical for the TE- and TM-excited modes, and their difference must be taken into account when designing practical polarization-independent filters.

The behavior as a function of duty cycle is more interesting at the conical angular orientation. Figure 7(a) shows the results for a grating duty cycle of 50%. Here there is a small spectral deviation (a small frequency gap) between the resonances of the two orthogonal polarizations. The peak reflection efficiency for one polarization is 84%, and the other is 99%, i.e., incomplete polarization independence. Yet, even with this nonoptimized GWS of 50% grating duty cycle, near-polarization-independent resonance is obtained.

Figure 7(b) shows the results of a grating duty cycle of 41.63%, for which there is no angular band gap, as evident in Fig. 5(b). Here the near-polarization-independent behavior is somewhat inferior to that shown in Fig. 7(a), as is evident from larger changes in peak reflection efficiencies of 99.5% for one polarization and 74% for the orthogonal polarization. Again, neither polarization reaches 100% reflection efficiency because the optimized angular orientation for this wavelength and duty cycle was not at the crossing. We found that at the exact crossing, the near-polarization-independent behavior is similar, where one polarization yields 100% reflection efficiency and the orthogonal polarization yields a lower reflection efficiency of 69% at a slightly lower wavelength. We presume that although there is no angular bandgap, only one TE–TM linear combination can be fully excited, as there is only one wavelength at the angular orientation of the crossing for which 100% reflection efficiency is possible. The other combination can be only partially excited. This second combination is the excitation responsible for the second peak at a slightly lower wavelength. For an incident light polarization of $(\alpha,\beta)=(-89°,1°)$, the reflection efficiency of this second peak reaches 99.7%. Thus, the optimal po-

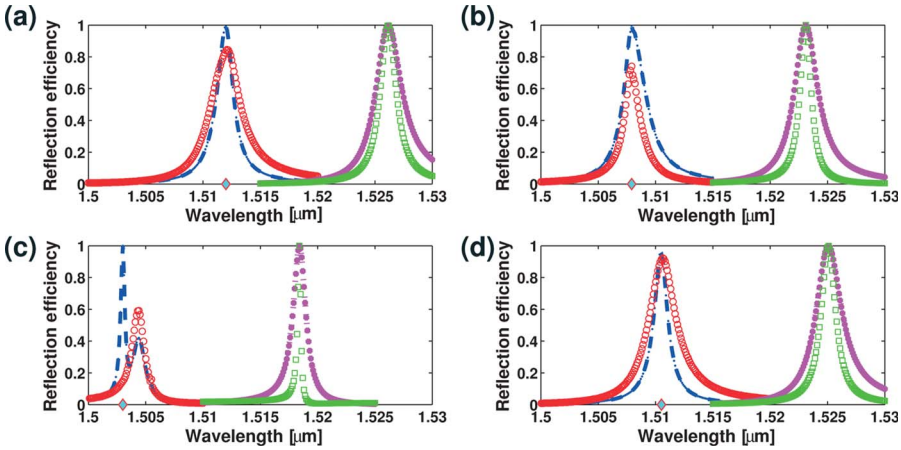

Fig. 7. (Color online) Numerically calculated reflection efficiency as a function of wavelength for four GWSs, each with a different grating duty cycle. The resonances at the higher wavelengths are for TE–TM crossing and classical angular orientations, where *s* polarization is denoted by the dotted curve and *p* polarization by squares. The resonances at the lower wavelengths are for TE–TM simultaneous excitations and the conical angular orientations marked by stars in Fig. 5, where the dashed curve denotes maximal polarization and the circles denote minimal polarization obtained from Fig. 6. (a) Grating duty cycle of 50%, (b) grating duty cycle of 41.63%, (c) grating duty cycle of 25%, (d) grating duty cycle of 47.2%.

larizations to excite the two different combinations of TE–TM-guided modes at the angular orientation of the crossing are not orthogonal.

Figure 7(c) shows the results for a grating duty cycle of 25%. Here there is no polarization-independent resonance at all, as is evident by the large spectral deviation between the two resonances relative to their bandwidths. For this duty cycle, maximal average reflection efficiency occurred at an angular orientation on one of the bands. Thus, the peak reflection efficiency of one resonance, at the wavelength denoted by the diamond, is 100%, while for the orthogonal polarization, the peak is much lower. These results, along with the results at the crossing for a grating duty cycle of 41.63%, differ from TE–TE and TM–TM resonances, where 100% reflection efficiencies can be obtained for two orthogonal polarizations. It should be noted that for this grating duty cycle of 25%, it is possible to obtain 100% reflection efficiency for the second peak as well, but this at a nonorthogonal polarization of $(\alpha,\beta)=(65°,-2°)$.

Figure 7(d) shows the result for a grating duty cycle of 47.2%, for which we obtained the optimum average reflection efficiency and near polarization independence. Specifically, the peak reflection efficiency of about 93% for both orthogonal polarizations is nearly constant and at very close wavelengths. Such optimized results are probably due to the fact that the polarizations on either side of the relatively small k gap are almost orthogonal, so that both polarizations still have high reflection efficiencies in the middle of the gap.

To summarize, we have shown that tunable near-polarization-independent resonance can be achieved when exciting TE–TM-guided modes simultaneously. At full conical incidence and classical incidence, resonances are always for *s*- and *p*-polarized light due to the fact that the resonances have well-defined symmetries. Efficient polarization-independent resonance will occur only if the *s* and *p* resonances occur at a specific angular orientation for two wavelengths that are much closer than the bandwidth of the resonances. This condition is met at full conical incidence over a tunable range only far from the normal incidence singularity and for specific duty cycles for which the photonic bandgap is small enough. At classical incidence, any GWS structure has a single angular orientation and corresponding wavelength for which there is complete polarization-independent resonance. This is true because at classical incidence, TE- and TM-guided modes do not interact, unlike counterpropagating TE–TE or TM–TM modes at full conical incidence. Thus there cannot be a photonic bandgap at classical incidence. The resonant wavelength can be tuned to a lower wavelength by changing θ_{CON}. However, at such angular orientations, TE–TM modes begin to interact, resulting in possible k gaps and frequency gaps. Moreover, since there is no defined symmetry of the plane of incidence in regard to the symmetry planes of the GWS, the resonant polarizations of the two bands on either side of the gap are not necessarily orthogonal, preventing complete polarization independence.

4. EXPERIMENTAL PROCEDURE AND RESULTS

In order to verify our calculations, we fabricated a 2 mm $\times$2 mm GWS with the same parameters used for the numerical calculations. The GWS substrate was of a high-quality, $\lambda/10$, BK7 glass plate. The waveguide layer was formed by spin coating an inorganic polymer OptInd 07, and the grating was formed by *e*-beam lithography in a poly (methyl methacrylate) (PMMA) layer and had a grating duty cycle of 50%.

The experimental arrangement for evaluating the GWS is schematically shown in Fig. 8. Our laser source is an Agilent (HP) 8164A tunable single-mode fiber laser, which was controlled by LabView through a GPIB protocol. The light from the fiber laser passed through a polarization wheel for controlling the incident polarization and was collimated. A part of the collimated beam was directed to

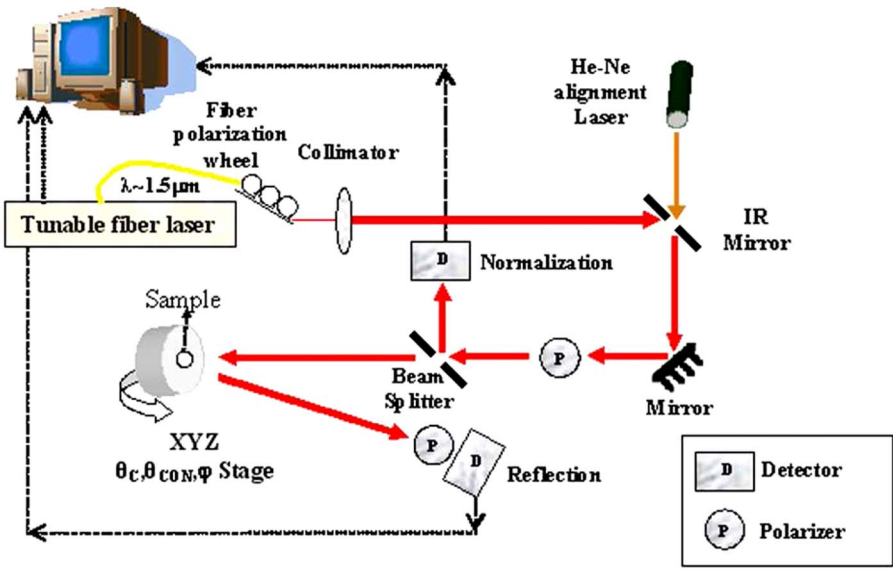

Fig. 8. (Color online) Experimental arrangement for measuring the reflection efficiency as a function of the incident wavelength, polarization, and angular orientation (θ_C, θ_{CON}).

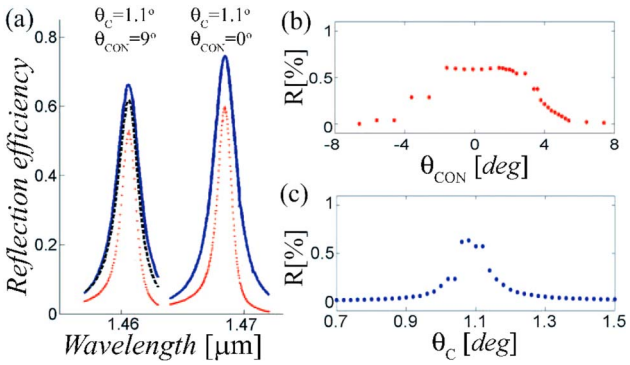

Fig. 9. (Color online) Experimental polarization-independent results. (a) Reflection efficiency as a function of wavelength at classical and off-classical incidence. Solid curve denotes *s*-polarized incident light, dotted curve *p*-polarized, and dashed curve 45° linearly polarized light. (b) Reflection efficiency as a function of the conical angle θ_{CON} (for a fixed wavelength). (c) Reflection efficiency as a function of the classical angle θ_C (for a fixed wavelength).

a detector connected to an Ophir LaserStar powermeter for normalization reference. The other part of the beam was incident onto the GWS sample. The GWS sample was set in *xyz* translation stages and rotating mounts for controlling the location and angular orientation of the incident beam with respect to the GWS sample, i.e., φ, θ_{CON}, and θ_C. The reflected light from the sample was measured by means of a second detector, aligned to detect the zero-order reflection. Placing an additional polarizer P adjacent to the second detector allowed for measurement of polarization conversion. At normal incidence, the second detector was oriented to detect the light reflected back through the beam splitter.

Representative experimental results are shown in Fig 9. Figure 9(a) shows reflection efficiency as a function of wavelength at a classical incidence of $\theta_C=1.1°$ and $\theta_{CON}=0°$ and at a specific conical incidence of $\theta_C=1.1°$ and $\theta_{CON}=9°$ for two orthogonal incident polarizations. As is evident, efficient polarization independence occurs at $\lambda=1.4607\ \mu$m and $\lambda=1.468\ \mu$m. The results confirm that it is indeed possible to tune the resonance wavelength for a single GWS just by selecting the proper angular orientation of the incident light. These results are qualitatively in agreement with the numerical results of Fig. 7(a). Figure 9(b) shows the reflection efficiency, $R[\%]$, as a function of the conical incidence angles, and Fig. 9(c) shows the reflection efficiency as a function of the classical incidence angle, both at $\lambda=1.468\ \mu$m (note the different scale along the abscissa). As is evident, at full conical incidence the angular tolerance is about 6°, much larger than the angular tolerance of about 0.15° at classical incidence, in agreement with the calculated results.

5. CONCLUDING REMARKS

To conclude, any GWS can have near polarization independence with TE–TM-guided-mode excitation over either a tunable range of wavelengths or a tunable range of incident angles. Such polarization independence is possible because TE–TM-excited guided modes do not interact at classical incidence for any GWS, so there is no photonic bandgap. The tunable range is dependent on the interaction between TE–TM modes at conical incidence, which generally results in k gaps and frequency gaps. In addition, the resonant polarizations of the two bands on either side of the gap are no longer orthogonal, thereby degrading polarization independence. This range can be maximized by tailoring the duty cycle. On the other hand, with TE–TE- and TM–TM-guided-mode excitation, polarization independence is possible only for specific GWSs where there are no photonic bandgaps and the angular orientation of the incident light is far from the resonance singularity at normal incidence.

Further theoretical and experimental research is needed to understand how the GWS parameters, such as the grating duty cycle, affect the k gap, the frequency gap, and the orthogonality of the two resonant polarizations at each edge of the band, so as to achieve near-polarization-independent resonance over a larger range of wavelengths and angular orientations of the incident light. Such research will allow us to further optimize the range of tunable near-polarization-independent resonance when TE–TM-guided modes are simultaneously excited and to fully understand the coupling processes involved.

ACKNOWLEDGMENTS

The authors would like to thank Michael Golub, David Rosenblatt, and Shmuel Blit for very helpful discussions.

REFERENCES

1. D. Rosenblatt, A. Sharon, and A. A. Friesem, "Resonant grating waveguide structures," IEEE J. Quantum Electron. **33**, 2038–2059 (1997).
2. D. Lacour, G. Granet, and J.-P. Plumey, "Polarization independence of a one-dimensional grating in conical mounting," J. Opt. Soc. Am. A **20**, 1546–1552 (2003).
3. G. Niederer, W. Nakagawa, and H. P. Herzig, "Design and characterization of a tunable polarization-independent resonant grating filter," Opt. Express **13**, 2196–2200 (2005).
4. A.-L. Fehrembach, D. Maystre, and A. Sentenac, "Phenomenological theory of filtering by resonant dielectric gratings," J. Opt. Soc. Am. A **19**, 1136–1144 (2002).
5. S. Peng and M. Morris, "Experimental demonstration of resonant anomalies in diffraction from two-dimensional gratings," Opt. Lett. **21**, 549–551 (1996).
6. A.-L. Fehrembach, A. Talneau, O. Boyko, F. Lemarchand, and A. Sentenac, "Experimental demonstration of a narrowband, angular tolerant, polarization independent, doubly periodic resonant grating filter," Opt. Lett. **32**, 2269–2271 (2007).

7. A. Mizutani, H. Kikuta, K. Nakajima, and K. Iwata, "Nonpolarizing guided-mode resonant grating filter for oblique incidence," J. Opt. Soc. Am. A **18**, 1261–1266 (2001).
8. A.-L. Fehrembach and A. Sentenac, "Study of waveguide grating eigenmodes for unpolarized filtering applications," J. Opt. Soc. Am. A **20**, 481–488 (2003).
9. A.-L. Fehrembach and A. Sentenac, "Unpolarized narrow-band filtering with resonant gratings," Appl. Phys. Lett. **86**, 1105–1108 (2005).
10. S. Soria, T. Katchalski, E. Teitelbaum, A. A. Friesem, and G. Marowsky, "Enhanced two-photon fluorescence excitation by resonant grating waveguide structures," Opt. Lett. **29**, 1989–1991 (2004).
11. N. Ganesh, I. D. Block, and B. T. Cunningham, "Near ultraviolet-wavelength photonic-crystal biosensor with enhanced surface-to-bulk sensitivity ratio," Appl. Phys. Lett. **89**, 316–328 (2006).
12. S. S. Wang and R. Magnusson, "Theory and applications of guided-mode resonance filters," Appl. Opt. **32**, 2606–2613 (1993).
13. I. Avrutsky and R. Rabady, "Waveguide grating mirror for large-area semiconductor lasers," Opt. Lett. **26**, 989–991 (2001).
14. T. Katchalski, G. Levy-Yurista, A. A. Friesem, G. Martin, R. Hierle, and J. Zyss, "Light modulation with electro-optic polymer-based resonant grating waveguide structures," Opt. Express **13**, 4645–4650 (2005).
15. P. S. J. Russell, "Optics of Floquet–Bloch waves in dielectric gratings," Appl. Phys. B: Photophys. Laser Chem. **39**, 231–246 (1986).
16. R. Zengerle, "Light propagation in singly and doubly periodic planar waveguides," J. Mod. Opt. **34**, 1589–1617 (1987).
17. M. G. Moharam, E. B. Grann, D. A. Pommet, and T. K. Gaylord, "Formulation for stable and efficient implementation of the rigorous coupled-wave analysis of binary gratings," J. Opt. Soc. Am. A **12**, 1068–1076 (1995).
18. GSolver, Grating Solver Development Company, http://www.gsolver.com.
19. F. Lemarchand, A. Sentenac, and H. Giovannini, "Increasing the angular tolerance of resonant grating filters with doubly periodic structures," Opt. Lett. **15**, 1149–1151 (1998).
20. J. D. Joannopoulos, R. D. Meade, and J. N. Winn, *Photonic Crystals — Molding the Flow of Light* (Princeton U. Press, 1995).
21. W. L. Barnes, T. W. Preist, S. C. Kitson, and J. R. Sambles, "Physical origin of photonic energy gaps in the propagation of surface plasmons on gratings," Phys. Rev. B **54**, 6227–6244 (1996).
22. D. Lacour, J.-P. Plumey, G. Granet, and A. M. Ravaud, "Resonant waveguide grating: Analysis of polarization independent filtering," Opt. Quantum Electron. **33**, 451–470 (2001).
23. D. Heitmann, N. Kroo, C. Schulz, and Z. Szentirmay, "Dispersion anomalies of surface plasmons on corrugated metal–insulator interfaces," Phys. Rev. B **35**, 2660–2666 (1987).
24. E. Popov, "Plasmon interactions in metallic gratings: w- and k-minigaps and their connection with poles and zeros," Surf. Sci. **222**, 517–527 (1989).
25. P. Tran, V. Celli, and A. A. Maradudin, "Conditions for the occurrence of k gaps for surface polaritons on gratings," Opt. Lett. **13**, 530–532 (1988).
26. A.-L. Fehrembach, S. Hernandez, and A. Sentenac, "k gaps for multimode waveguide gratings," Phys. Rev. B **73**, 233405 (2006).